



Refined spatiotemporal analysis of drought characteristics under different characteristic variable matchings: a case study of the middle reaches of the Yellow River basin, China

Ying Li^{1,2} · Chenchen Jia¹ · Shuang Ma¹ · Zhentai Hu¹ · Jin Sun¹

Received: 30 December 2021 / Accepted: 4 April 2022 / Published online: 14 April 2022
© The Author(s), under exclusive licence to Springer-Verlag GmbH Germany, part of Springer Nature 2022

Abstract

The refined assessment of the spatiotemporal characteristics of droughts is of great significance for drought evaluation. Based on monthly precipitation and temperature grid data (1961–2019) in the middle reaches of the Yellow River basin (MYRB), the standardized precipitation evapotranspiration index (SPEI) was calculated at monthly, seasonal, and annual scales. The run theory was used to extract the drought features at the monthly scale, and the spatiotemporal characteristics of different drought levels were analyzed using Mann–Kendall mutation tests and spatial interpolation. The Moran' I was used to analyze the spatial heterogeneity of droughts. The results showed that the drought trend in the MYRB increased from 1961 to 2019, with the SPEI exhibiting an overall decreasing rate of $-0.1145/\text{decade}$. Decreasing rates were observed in spring ($-0.1356/\text{decade}$), summer ($-0.0362/\text{decade}$), and autumn ($-0.0745/\text{decade}$), whereas an increasing rate was observed in winter ($0.0781/\text{decade}$). Only extreme droughts were long term, with an intensity as low as -22.29 . The highest frequencies were observed for mild–moderate droughts, which mainly showed high-value clusters in the western and central regions. The frequencies of severe–extreme droughts mainly presented low-value clusters in the northern and southwestern areas. The frequencies of mild and severe droughts exhibited significant spatial cluster characteristics, while the drought intensity showed non-significant spatial clusters and a random distribution. The high and low values of drought intensity were mainly clustered in the middle–upper reaches. The research results provide reference for disaster prevention and mitigation, agricultural planning, and water resource allocation in the MYRB.

Keywords SPEI; MYRB · Run theory · Spatiotemporal evolution · Moran's index · Refined

Introduction

Of all natural disasters worldwide, drought has the longest duration and some of the most significant impacts and harmful effects (Hao et al. 2014; Rajsekhar et al. 2015). According to statistics, worldwide, drought accounted for 34% of disaster related deaths (650,000 deaths) from 1970 to 2019 (World Meteorological Organization (WMO) 2020) and caused global economic losses of $\$1.75 \times 10^{12}$ from 1900 to 2019. Since the 1950s, climate warming and drying have increased the frequency, intensity, and scope of drought events in China, severely affecting agricultural production, the ecological environment, and socio-economic development (Hu et al. 2021; Cook et al. 2015; Xu et al. 2015). The drought-affected area and food loss showed overall increasing trends from 1951 to 2013. In 2000, the drought-affected area and yield of

Responsible Editor: Philippe Garrigues

Highlights

- Spatiotemporal distribution characteristics of droughts in the middle reaches of the Yellow River basin (1961–2019) were effectively analyzed using grid data.
- The frequency and intensity of drought in the middle reaches of the Yellow River basin were higher in the south and lower in the north.
- The spatial patterns of drought frequency and intensity mainly showed clusters and a random distribution.

✉ Ying Li
liying@lnnu.edu.cn

¹ School of Geography, Liaoning Normal University, Dalian, China

² Liaoning Key Laboratory of Physical Geography and Geomatics, Liaoning Normal University, Dalian, China

crops were 2.7×10^7 ha and 5.996×10^{10} kg, respectively (Yu et al. 2014; Zhang et al. 2019). In China, severe and extreme droughts mainly occur in North China and in the Yellow River and Huai River basins (Zhang et al. 2019). Under the combined effect of climate change, the Asian Monsoon system, and human activities in the Yellow River basin, extreme climate conditions, especially droughts, have been increasing in frequency and intensity (Omer et al. 2020). The World Meteorological Organization has emphasized that the refined description of the spatiotemporal distribution of drought has an important impact on alleviating regional drought and formulating and implementing national policies (World Meteorological Organization (WMO) 2007, 2019). Refinement is the use of regional tools to either refine or reduce climate information and then the use of high-resolution spatiotemporal data to analyze regional or local scale climate changes (Giorgi 2008; Zhao et al. 2020). However, the resolution of spatiotemporal data currently used in many areas is insufficient, making it difficult to refine and effectively evaluate drought events (Hong et al. 2021; Pachauri and Reisinger 2007; Xu et al. 2020). Therefore, the effective identification of drought events and the refined assessment of the spatiotemporal evolution characteristics of different types of droughts are particularly urgent.

To analyze the spatiotemporal characteristics of regional drought events, it is necessary to select appropriate drought indicators based on the collection of meteorological data and then use appropriate statistical methods to determine the corresponding spatiotemporal trends and correlations. First, meteorological data include station data and grid data. Although station data can effectively capture the rapid changes in meteorological parameters, they can only represent the meteorological conditions around the meteorological station (i.e., spatially limited). Grid data involve the use of interpolation to transform site data into spatial resolutions, which is a more flexible approach. However, spatial interpolation may be affected by the number and density of meteorological stations as well as topography, thus affecting the accuracy of interpolation (Arshad et al. 2021). Compared with station data, grid data refine meteorological data spatially, making the spatial distribution more uniform and continuous. Second, the drought index is the basis and tool for drought monitoring and research. The commonly used classic drought indicators are the Palmer Drought Severity Index (PDSI), standardized precipitation index (SPI), standardized precipitation evapotranspiration index (SPEI), crop water index (Z index), and comprehensive meteorological drought index (CI index) (Palmer 1965; McKee et al. 1993; Lhotka et al. 2020; Palmer and Wayne 1968; Sun et al. 2013). Among them, the SPEI compensates for

the shortcomings of the SPI, which neglects the impact of evapotranspiration on drought, has a fixed PDSI time-scale, and requires many parameters (Guo et al. 2017; Vicente-Serrano et al. 2010; Tirivarombo et al. 2018; Zhao et al. 2017). The SPEI is widely used in many fields because it is more flexible and improves the accuracy of drought monitoring and research compared with other methods. Numerous methods have been developed and used to accurately identify drought events and characterize the spatiotemporal distribution characteristics of drought durations, intensities, impact ranges, and periods. These methods include the threshold method (Hisdal et al. 2004), run theory (Ayantobo et al. 2017), empirical orthogonal function (Wang et al. 2015), wavelet analysis (Yerdelen et al. 2021), principal component analysis (Son et al. 2021), and spatial autocorrelation. Owing to its simple operation and the advantages of quantitative statistics of drought duration, frequency, and intensity, run theory has become the simplest and most common method to describe the spatiotemporal distribution characteristics of drought. Spatial autocorrelation is used to test whether certain attributes of spatial elements and adjacent elements are spatially dependent, and the commonly used approach is Moran's index (Moran's I) (Kumari et al. 2019). The global Moran's I can describe whether drought characteristics are spatially dependent (Prudhomme et al. 2014), while the local Moran's I can evaluate the spatial agglomeration characteristics of drought features (Mishra and Singh 2010). Previous descriptions of the spatial distribution characteristics of drought events lacked refined and comprehensive research. In drought monitoring and drought spatiotemporal descriptions, scholars have over-emphasized the spatiotemporal evolution of drought frequency and intensity, while ignoring the spatial distributions of the frequencies and intensities of drought events of different durations (Zhai et al. 2017). In addition, few studies have performed correlation analyses of the spatial distributions of drought characteristics.

The middle reaches of the Yellow River basin (hereafter "MRYB") are important production bases for agriculture and animal husbandry in China. However, water resources are unevenly distributed, and the amount of water resources per capita in some areas is only 530 m³, which is one-sixth of the global average per capita water resource (Chen et al. 2020). The contradiction between supply and demand is prominent, which seriously restricts agricultural production and regional economic development. Between 1956 and 2016, the MRYB became much warmer and drier, and the worst drought occurred in 1997. The annual mean temperature has increased by 0.26 °C per decade, and the annual precipitation has decreased by 10.9 mm per decade (Bao et al. 2019). There is an increase in the contribution of

potential evapotranspiration to severe droughts owing to the global warming and arid to semi-arid climate in the MYRB (Wang et al. 2021). The impact of global climate change has led to an increase in drought frequency potential and drought intensity and longer drought duration (Han et al. 2021). And the drought has become regionally significant. To evaluate the drought characteristics in the MYRB more precisely than previously achieved, the precipitation and temperature data of 185 grid points in the region were collected in this study. Then, the drought level was quantitatively analyzed using the SPEI, and the temporal evolution characteristics of the SPEI at seasonal and interannual scales were analyzed by linear trend analyses and Mann–Kendall (M–K) mutation tests. The run theory was used to identify drought events, and the spatial distributions of the frequencies and intensities of different drought levels were determined based on their characteristic variables. Droughts were divided into short-term, medium-term, and long-term drought events based on their durations, and the spatial distributions of the frequencies and intensities of each group were analyzed. In addition, Moran's I was used to explore the overall and local correlation characteristics of the frequencies and intensities of different drought levels. The purpose of this research is to analyze the spatiotemporal changes of different types of droughts in the MYRB in a detailed manner, thus providing a basis for relevant departments to deal with different drought characteristics and adjust drought response strategies between regions.

Study area and methods

Study area

The MYRB (33.69°N–41.42°N, 103.75°E–113.75°E) is the river section from Hekou Town in Tuoketuo County (Inner Mongolia) to Taohuayu in Zhengzhou City (Henan Province) (Fig. 1). It has a total length of 1234 km and a drainage area of 362,000 km² and includes the provincial administrative regions of Shaanxi, Shanxi, Henan, Inner Mongolia, Ningxia, and Gansu. The MYRB is a transition zone from a semi-humid climate to an arid–semi-arid climate (Fig. 2a) and includes an arid–semi-arid desert area of the Loess Plateau and Ordos Plateau. Precipitation varies considerably over a year, and the mean annual precipitation is 518 mm, which is mainly concentrated in July, August, and September (Fig. 2b). Higher temperatures in spring and summer lead to higher annual evapotranspiration (Fig. 2c). The mean annual evaporation is 1055 mm. Gansu, Ningxia, and the central and western regions of Inner Mongolia have the largest annual evaporation amounts in China, with the maximum annual evaporation exceeding 2500 mm (Bao et al. 2019). Due to the uneven spatiotemporal distribution of precipitation and high evapotranspiration, water shortage is a serious issue. During the critical period of agricultural water use, the drought trend is aggravated because the water shortage rate continues to rise (Peng et al. 2019). The ecological–geological environment in the MYRB is complex, with low vegetation coverage, serious

Fig. 1 Geographical location, elevation, and grid distribution of meteorological data of the study area

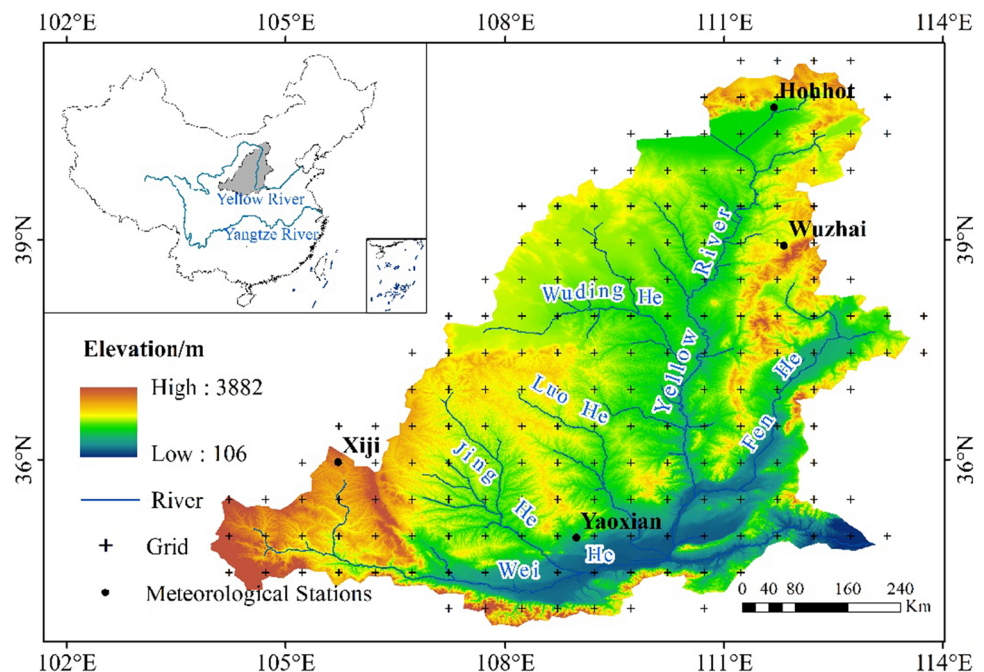
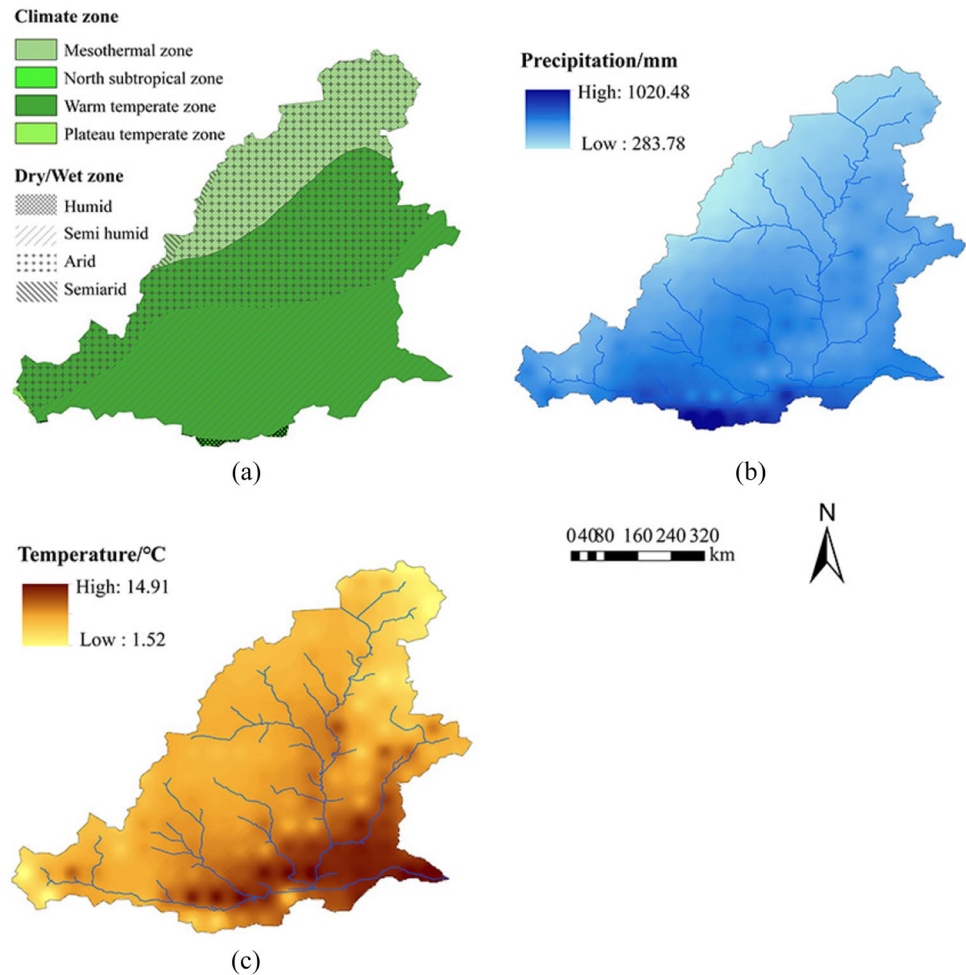


Fig. 2 (a) Climate zone and dry/wet zone, (b) mean annual precipitation, and (c) monthly mean temperature of the study area from 1961 to 2019



soil erosion, and complicated climatic conditions (Xu et al. 2021a, b; Wu et al. 2018).

Data sources

The precipitation and temperature data used in this study were monthly grid data provided by the National Meteorological Science Data Center (<http://data.cma.cn>). The data covered the period from 1961 to 2019 and had a total of 185 grid points with a spatial resolution of $0.5^\circ \times 0.5^\circ$. The grid dataset adopts thin-disk spline interpolation specifically for climate data and simultaneously introduces digital elevation data. The cross-validation method was used to control data quality. The timeseries of the data was compiled, and the quality was found to be good. Elevation data were obtained from the Geospatial Data Cloud (<http://www.gscloud.cn>) SRTMDEM 90-m resolution product. Based on ArcGIS hydrological analysis tools, the hydrological extraction method was used to calculate the confluences, raster river network vectorization,

and subbasins in the MYRB to extract hydrological information such as the river network distribution and basin boundaries.

Research methods

Drought index

The drought index is an important indicator for quantitatively identifying drought characteristics. The MYRB is an arid–semi-arid region, and the SPEI considering evapotranspiration has good applicability for the study of drought characteristics in this area. The SPEI is a commonly used index for evaluating meteorological drought events. Droughts at different timescales can be evaluated by calculating the difference between precipitation and evapotranspiration. The calculation method of the SPEI refers to the explanation provided by Zhao et al. (2017).

- 1) Use Thornthwaite method to calculate potential evapotranspiration (PET):

$$PET = \left(\frac{2uN}{45}\right)\left(\frac{10T_i}{I}\right)(6.75 \times 10^{-7})I^3 - (7.71 \times 10^{-5})I^2 + (1.79 \times 10^{-2})I + 0.49 \tag{1}$$

where u is monthly average daily sunshine hours of the i -th month, N is total days of the i -th month, T_i is monthly average temperature, and I is the heat index.

- 2) Calculate the difference between precipitation and evapotranspiration:

$$D_i = P_i - PET_i \tag{2}$$

- 3) Normalize the D_i data sequence and find the SPEI to which each data point corresponds. Because there may be negative values in the original data sequence D_i , the SPEI uses the three-parameter log-logistic probability distribution, $F(x)$, as

$$F(x) = \left[1 + \left(\frac{\alpha}{x + \gamma}\right)^\beta\right]^{-1} \tag{3}$$

P is the probability of a definite D value:

$$P = 1 - F(x) \tag{4}$$

For $P \leq 0.5$,

$$w = \sqrt{-2\ln(P)},$$

$$SPEI = w - \frac{c_0 + c_1w + c_2w^2}{1 + d_1w + d_2w^2 + d_3w^3} \tag{5}$$

where $C_0 = 2.515517$, $C_1 = 0.802853$, $C_2 = 0.010328$, $d_1 = 1.432788$, $d_2 = 0.189269$, and $d_3 = 0.001308$.

In the present study, the SPEI-1, SPEI-3, and SPEI-12 were used to represent the drought conditions in a month, season, and year, respectively. The drought level refers to the categorization of GB/T20481-2017, which divides drought events into five levels (Table 1).

Table 1 SPEI ranges corresponding to different drought levels

Level	SPEI	Type
1	$(-\infty, -0.5)$	No drought
2	$(-1, -0.5]$	Mild drought
3	$(-1.5, -1]$	Moderate drought
4	$(-2, -1.5]$	Severe drought
5	$[-2, +\infty)$	Extreme drought

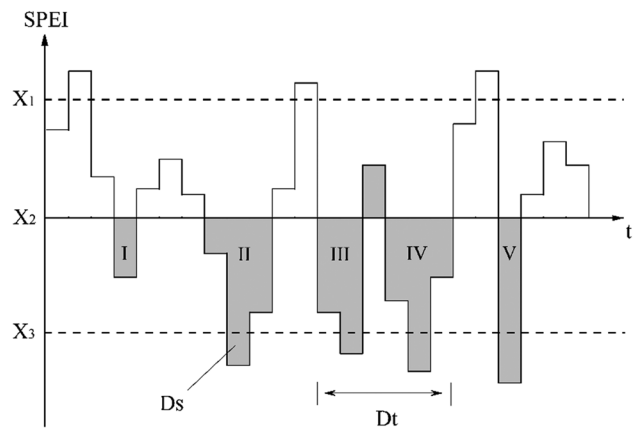


Fig. 3 Schematic diagram of the run theory

Drought identification

The run theory was used to identify drought events and assess the drought levels in the MYRB. The threshold for statistical drought conditions was set to X_1 , X_2 , and X_3 . When the drought index was $< X_2$, it was judged as a drought event. As shown in Fig. 3, there were five drought events: I, II, III, IV, and V. When the drought lasted for only one period (e.g., I, V) and the drought index value was $< X_3$ (e.g., V), it was judged as a drought event; otherwise, it was not counted as a drought event. For two adjacent drought events (e.g., III and IV) with an interval of one period, if the drought index of the interval was $< X_1$, these two adjacent droughts were regarded as one drought event; otherwise, there were treated as two independent droughts. The combined drought duration was $Dt = D_{III} + D_{IV} + 1$, and the drought intensity was $Ds = SPEI_{III} + SPEI_{IV}$. According to the above rules, there are three drought processes in Fig. 3, namely II, III + IV, and V (Ayantobo et al. 2017). As the drought intensity value is negative, the severity of the degree of drought increases with a decrease in the drought intensity value. As shown in Table 1, the level of a drought event was determined according to the maximum SPEI of the event. Based on the SPEI-1 and drought level threshold (Table 1), the run theory was used to count the frequencies, intensities, and durations of different drought levels. Drought duration is an important characteristic for measuring the severity of a drought event and was divided into three grades as follows. A drought that lasts for 1–3 months was regarded as a short-term drought (Zhai et al. 2017), while a drought that lasts for 4–12 months was considered to be a medium-term drought, and a drought that lasts longer than 12 months was regarding as a long-term drought. On this basis, the drought frequency and intensity were analyzed to fully explore the drought characteristics in

Table 2 Drought type based on drought level and duration

Type	Drought level			
	Mild drought	Moderate drought	Severe drought	Extreme drought
Short term (1–3 months)	S-Mi	S-Mo	S-S	S-E
Medium term (4–12 months)	M-Mi	M-Mo	M-S	M-E
Long term (> 12 months)	L-Mi	L-Mo	L-S	L-E

the MYRB. Considering the different levels and durations, there were 12 types of droughts (Table 2).

Analysis of spatiotemporal characteristics

Trend analysis and the M–K mutation test were used to analyze the temporal characteristics of drought events in the MYRB. Linear trend analysis is commonly used to analyze the linear trend of the independent variable x and dependent variable y . Therefore, the univariate linear regression analysis method was used to quantitatively analyze the changing trend of the SPEI. The calculation formula refers to the linear regression analysis of Yang et al. (2018). The M–K mutation test is a non-parametric test method that is widely used in meteorological and hydrological drought monitoring. Under the M–K mutation test, the positive sequence (UF) and inverse sequence (UB) were constructed; the change trend and mutation characteristics of the sequence were assessed according to the positive sequence (UF). When the intersection point of the UF and UB curves fell between the two confidence lines (± 1.96), then the time corresponding to the intersection point was considered as the time when the mutation began. The significance was judged by whether the statistic $|Z|$ exceeded ± 1.96 . The calculation formula is given in Li et al. (2021).

The inverse distance weighting method was used to perform spatial interpolation of each element to realize spatial visualization. Moran's I was used to analyze the overall and local correlation characteristics of the frequencies and intensities of different drought levels. As mentioned, Moran's I is divided into the global Moran's I and the local Moran's I . Spatial autocorrelation can be further divided into positive and negative spatial correlations. A positive spatial correlation refers to the observed value, which has high or low values that are similar to those of its neighbor, that is, there is spatial clustering. In contrast, a negative spatial correlation indicates different spatial outliers around the observed values. The global Moran's I is between -1 and 1 , whereby the closer the value is to 1 , the more significant the spatial agglomeration effect of an attribute in a geographical element (i.e., the spatial positive correlation). The closer the index value is to -1 , the more significant the spatial divergence of an attribute in a geographical element (i.e., the spatial negative correlation). An index value of 0 indicates no correlation (i.e., a random distribution). The

calculation formula refers to that of Kumari et al. (2019). The global Moran's I can only analyze whether geographical elements are spatially correlated as a whole and cannot analyze which other elements are correlated with geographical elements or where they are located. The local Moran's I is based on the global Moran's I and is used to spatially characterize whether there is high-value or low-value local spatial agglomeration in the region. There are four types of spatial correlation between observations and adjacent values, including two spatial clustering types: high values in a high-value neighborhood (high–high, H–H), low values in a low-value neighborhood (low–low, L–L), and two spatial discrete types (outliers): a high value surrounded by low values (high–low, H–L) and a low value surrounded by high values (low–high, L–H).

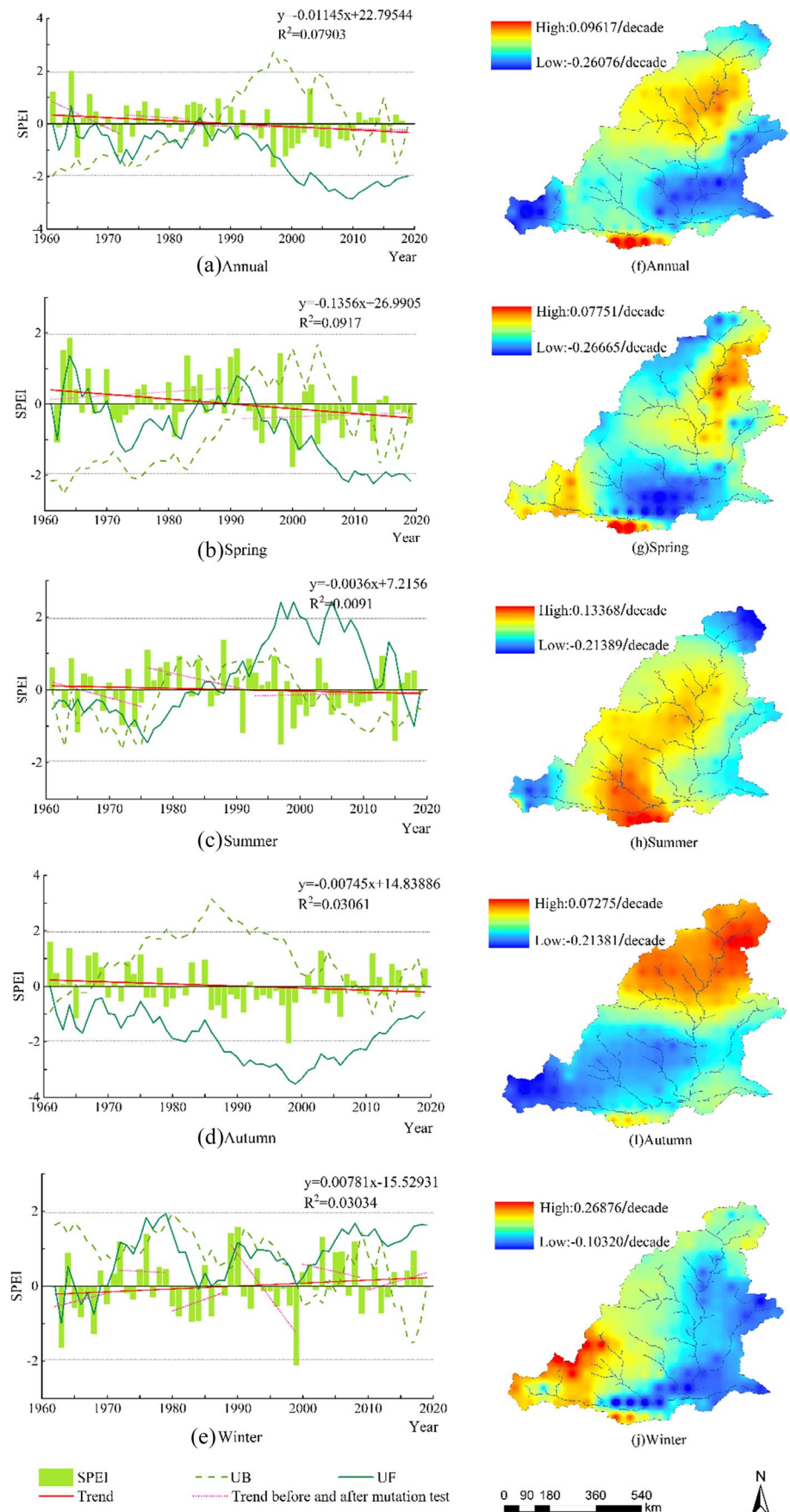
Results

SPEI trends and mutations

The linear trend and M–K mutation tests were used to describe the temporal trend of the SPEI in the MYRB (Fig. 4). Annually, the SPEI fluctuated considerably from 1961 to 2019 and exhibited an overall decreasing rate of $-0.1145/\text{decade}$ (Fig. 4a). The SPEI values in 1965, 1972, 1997, and 1999 were -1.28 , -1.08 , -1.65 , and -1.22 , respectively. The MYRB experienced 10 mild droughts, 3 moderate droughts, and 1 severe drought from 1961 to 2019. The node of the SPEI was 1985, whereby 1961–1985 was relatively wet and 1985–2019 was relatively dry.

Seasonally, the SPEI decreased at a rate of $-0.1356/\text{decade}$ in spring (1961–2019), which was the most significant downward trend of the seasonal trends. The lowest SPEI (-1.76) occurred in the spring of 2000 (Fig. 4b). In summer, the SPEI decreased at a rate of $-0.0362/\text{decade}$, which was not an obvious downward trend (Fig. 4c). Within this, the summertime SPEI decreased during 1961–1978, increased during 1979–1990, and decreased during 1991–2019. It was relatively humid during 1976–1996 and relatively dry during 1997–2015 (Fig. 4d). In autumn, the SPEI decreased at a rate of $-0.0745/\text{decade}$ and was low from 1997 to 2015. The lowest autumn time SPEI (-2.04) was observed in 1998 coinciding with an extreme drought. In winter, the SPEI fluctuated but increased at a rate of $0.0781/\text{decade}$ (i.e.,

Fig. 4 Variation trend and mutation test of the SPEI in the MYRB from 1961 to 2019 (a–e are the temporal trends and abrupt changes of the SPEI, and f–j are the spatial trends of the SPEI)



winters were humid) (Fig. 4e). The winters of 1961–1968 and 1980–1987 belonged to drought periods, and the lowest SPEI (-2.11) was observed in 1998, indicating extreme drought conditions.

On an annual scale, there were six mutations in the SPEI (Fig. 4a). The most obvious mutation was in 1985. The downward trend of the SPEI from 1985 to 2010 was significant, indicating that the aridification trend intensified during this period. In spring, the SPEI experienced a sudden change in 1992 and exhibited significant ($P < 0.05$) downward trends in 2008–2009, 2011–2015, and 2016–2019 (Fig. 4b). The mutation curve of the SPEI fluctuated considerably in summer, with multiple mutations; however, the mutation curve did not pass the significance test ($P > 0.05$; Fig. 4c). The mutation curves of the SPEI in autumn were all below 0. The mutation occurred in 1962, and the significance test was passed from 1987 to 2011 ($P < 0.05$), and the drought trend was significant (Fig. 4d). The mutation curve of the SPEI fluctuated greatly in winter, and there were multiple mutations from 1970 to 2010, alternating between dry and wet conditions.

Regarding the spatial distribution of the seasonal variation trends of the SPEI, declining drought conditions were most significant in the MYRB in spring, especially in the Jinghe and Luohe basins, with the highest declining rate of $-0.2667/\text{decade}$ (Fig. 4g). In summer, the most significant decreasing trend of the SPEI was observed in the northern part of the MYRB, reaching $-0.2139/\text{decade}$, while the SPEI values in the central and northern regions showed increasing trends (Fig. 4h). In autumn, the SPEI exhibited an increasing trend in the northern area of the MYRB, whereas a decreasing trend was observed in the southern area (Fig. 4i). Among these areas, the Weihe River basin had the most significant declining trend, reaching $-0.2138/\text{decade}$. In winter, a significant rising trend in the SPEI was only observed in the middle–upper reaches of the Weihe River basin, reaching $0.2688/\text{decade}$ (Fig. 4j). The downward trends in other regions were not evident, and the minimum declining rate of the SPEI was $-0.1032/\text{decade}$.

Characteristics of drought events

Drought frequency

The spatial distribution characteristics of drought frequency in the MYRB from 1961 to 2019 are described in Fig. 5. Overall, the drought frequency in the south of the MYRB was high, with the upper reaches of the Jinghe River basin recording the highest frequency of 192 droughts. The drought frequency in the north of the MYRB was low, with the north of the Wudinghe River basin recording the lowest frequency of 101 droughts.

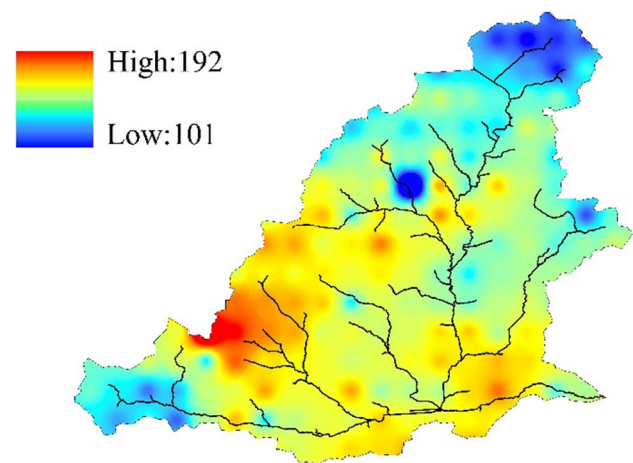
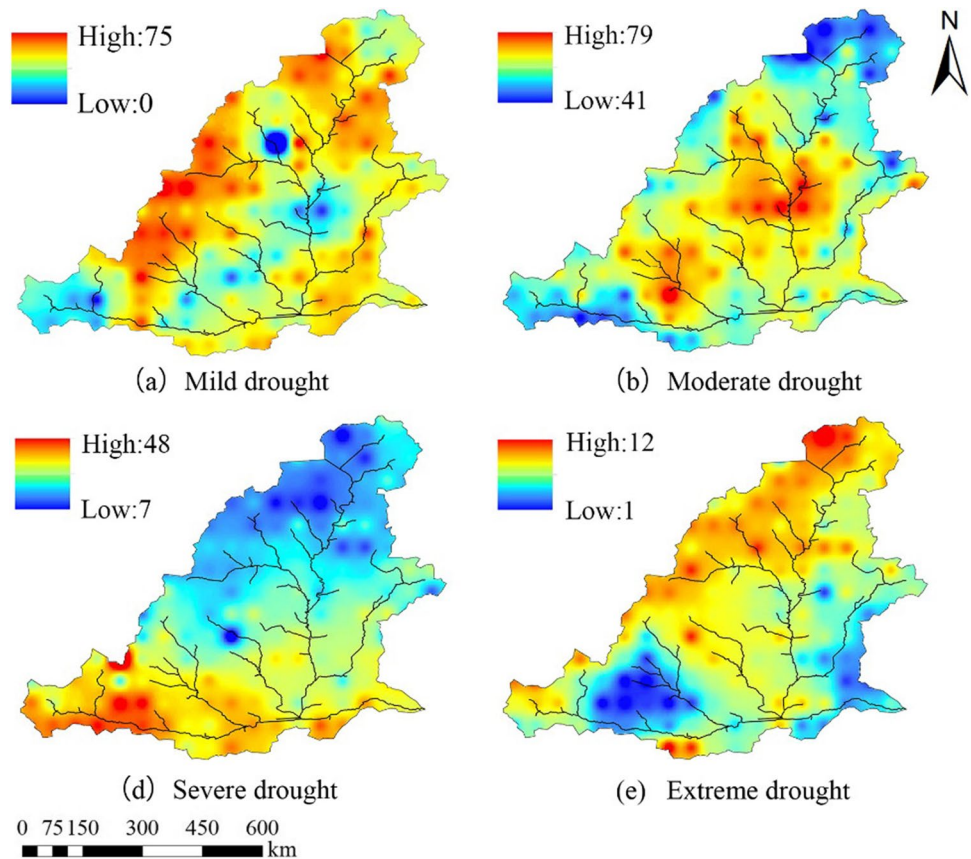


Fig. 5 Spatial distribution of total drought frequency in the MYRB from 1961 to 2019

Spatially, the frequencies of different drought levels varied within the MYRB during 1961–2019. The frequency of mild droughts was generally higher than those of the other levels. With an increase in the drought level (i.e., from mild to extreme), the drought frequency gradually decreased. The frequency of mild droughts (Fig. 6a) ranged from 40 to 75 in the subbasins of the MYRB, with the highest frequency of 75 observed in the upper reaches of the Wudinghe River basin, which then reduced to 40–50 in its lower reaches, the middle reaches of the Luohe River basin, the middle reaches of the Jinghe River basin, and the upper reaches of the Weihe River basin. Moderate droughts (Fig. 6b) were concentrated in the middle of the MYRB, especially in the Jinghe and Wudinghe basins, with a frequency of 60–79. The frequency of moderate droughts in the northern part of the MYRB and in the Weihe River basin was lower but still > 40 . The frequency of severe droughts (Fig. 6c) decreased from the south (maximum of 48 in the Weihe River basin) to the north (< 20). The frequency of extreme droughts (Fig. 6d) was highest in the north (12) and lowest in the southern areas of the Weihe and Fenhe basins (1–3).

According to the drought type, 93.5% of droughts in the MYRB were short-term droughts lasting 1–3 months. The frequency of S–S droughts was the highest (78). Regarding mid-term droughts (4–12 months), the frequencies of M–Mo droughts and M–S droughts were the highest (8). Among long-term droughts (> 12 months), only extreme drought lasted longer than 12 months, and it had a frequency of 1 in the given study period (Fig. 7). By analyzing the drought frequencies of the 12 types of droughts (i.e., based on different durations and levels; Table 2), the highest frequency of S–Mi droughts was observed in the upper reaches of the Jinghe and Wudinghe basins (> 60 ; Fig. 7a). For M–Mi droughts, the highest frequency was in the Jinghe and

Fig. 6 Spatial distribution of drought frequency in the MYRB from 1961 to 2019



Wudinghe basin (up to two; Fig. 7b). S-Mo droughts were concentrated in the Jinghe, Luohe, and Wudinghe basins, with most occurring in the Jinghe River basin (78; Fig. 7c). The high-frequency area of M-Mo droughts was the Fenhe River basin (eight; Fig. 7d). The high-frequency area of S-S droughts included the Weihe, Jinghe, and Luohe basins, and decreased northwards. Among them, the Weihe River basin had the highest frequency (46; Fig. 7e). The high-frequency area of M-S droughts was mainly distributed in the northern part of the MYRB and in the Weihe River basin, with the latter having the highest frequency (eight; Fig. 7f). The high-frequency area of S-E droughts was in the Wudinghe and Jinghe basins, although the highest frequency was in the Wudinghe River basin (nine; Fig. 7g). M-E droughts occurred more frequently in the northern part of the MYRB (up to six; Fig. 7h). For L-E droughts, the highest frequency was one, which occurred in the Wudinghe and Fenhe basins, while 91% of the area of the MYRB did not experience an L-E drought (Fig. 7i).

Drought intensity

The spatial distribution characteristics of drought intensity in the MYRB from 1961 to 2019 are described (Fig. 8). Overall, the drought intensity in the south of the MYRB was

high, especially in the Jinghe River basin and Weihe River basin, with a maximum of -10.61 . The drought intensity in the north of the MYRB was low, with a minimum of -17.83 .

The spatial distribution of different levels of drought intensity in the MYRB from 1961 to 2019 was used to analyze the degree of drought (Fig. 9). The natural breakpoint method was used to classify high and low drought intensities. Where there was no drought, the drought intensity was recorded as 0.

The low-intensity area of mild droughts was mainly distributed in the Luohe River basin and the lower reaches and southwestern part of the Fenhe River basin, where the lowest drought intensity was -2.31 (Fig. 9a). The upper reaches of the Weihe River basin and the northern part of the Wudinghe River basin had higher intensities of mild droughts. The low-intensity areas of moderate droughts included the Luohe River basin, upper reaches of the Weihe River basin, and northern part of the MYRB. The Jinghe River basin had the lowest drought intensity of -4.48 (Fig. 9b). The intensity and frequency of severe droughts in the MYRB showed opposite spatial distributions (Figs. 4c and 6c). The intensity of severe droughts in the northern part of the MYRB was relatively low, with a minimum of -6.24 , whereas it was higher in the Luohe and Fenhe basins (Fig. 9c). The low-intensity areas of extreme droughts (Fig. 9d) were concentrated in

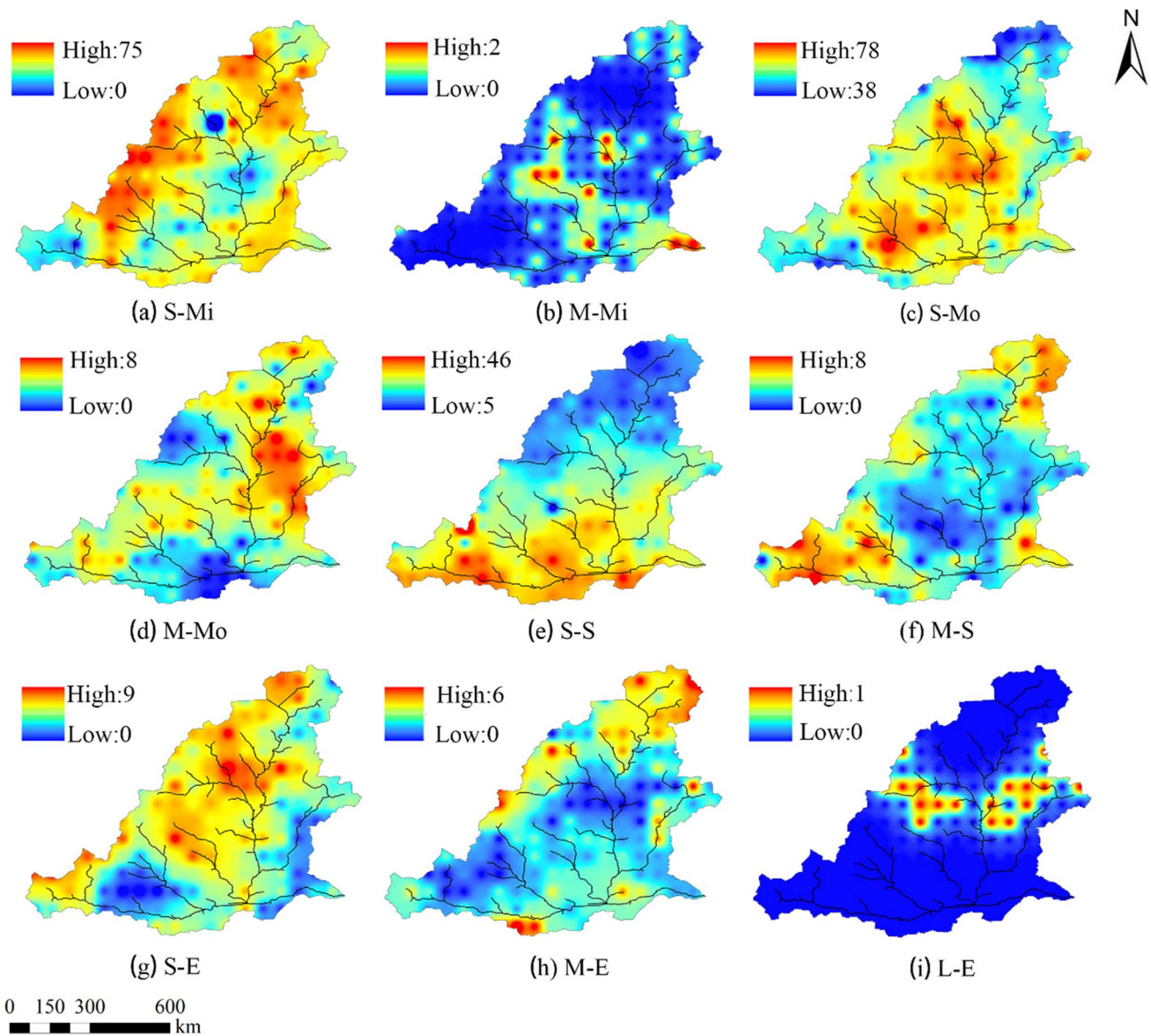


Fig. 7 Spatial distribution of the frequencies of different types of droughts (based on durations and levels) in the MYRB from 1961 to 2019

the northern part of the MYRB, the upper reaches of the Wudinghe River basin, and the upper reaches of the Fenhe River basin. The intensity of extreme droughts was relatively low in the Fenhe River basin, reaching -8.44 , whereas it was relatively high in the Weihe River basin, reaching -2.18 .

The spatial distribution of drought intensity for different types of droughts (i.e., based on durations and levels) was described to analyze the drought conditions in the MYRB from 1961 to 2019 (Fig. 10). The natural breakpoint method was used to classify the high and low drought intensities for different types of droughts. The intensity of S-Mi droughts was generally low (< -1.3) over 70% of the area of the MYRB. No S-Mi droughts occurred in the northern part of the Wudinghe River basin; hence, the drought intensity was

0 (Fig. 10a). The low-intensity areas of M-Mi droughts were concentrated in the southeastern part of the MYRB and in the Luohe River basin (minimum of -4.03 ; Fig. 10b). The low-intensity areas of S-Mo droughts were the Weihe and Jinghe basins, with the lowest intensity of -2.31 . The intensity of S-Mo droughts was generally high in the northern part of the Wudinghe River basin and the northern part of the Luohe River basin (minimum of -1.38 ; Fig. 10c). The high-intensity areas of M-Mo droughts were in the upper reaches of the Weihe, Luohe, and Wudinghe basins and in the northern part of the MYRB. The intensity of M-Mo droughts was < -5 , with the lowest being -7.34 (Fig. 10d). Figure 10e shows that the intensity of S-S droughts was high in most areas where the river passed through, while it was

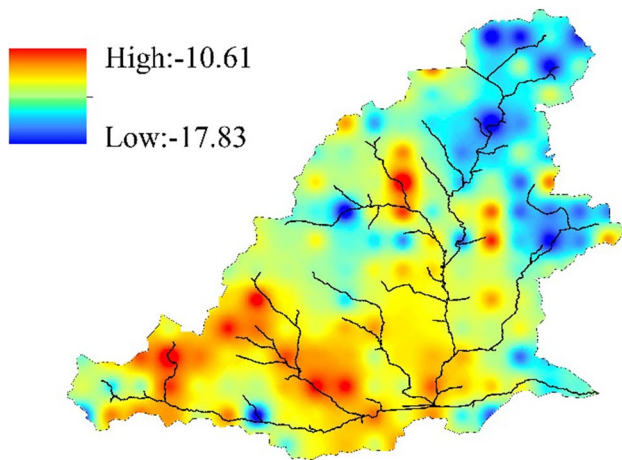


Fig. 8 Spatial distribution of total drought intensity in the MYRB from 1961 to 2019

lower in the northern part of the Wudinghe River basin and in the upper reaches of the Jinghe River basin (minimum of -3.48). The intensity of M-S droughts was relatively high in the south (e.g., the Luohe River basin and the middle reaches of the Fenhe River basin) and low in the north, with the lowest intensity of -10.56 occurring in the northwestern part of the MYRB (Fig. 10f). Overall, the intensity of S-E droughts gradually increased from the northeast to the southwest, and the lowest intensity (-4.75) was observed in the southeast (Fig. 10g). Figure 10h shows that no M-E droughts occurred in the southern part of the Wudinghe River basin, northern part of the Fenhe River basin, and the

upper reaches of the Weihe River basin. The lowest intensities of M-E droughts were observed in the northern and southern parts of the MYRB, with a minimum of -13.4 in the north. The lowest intensity of L-E droughts (-22.29) was observed in the upper reaches of the Fenhe River basin, while the highest intensity (-14.7) occurred in the southern part of the Wudinghe River basin (Fig. 10i).

Spatial heterogeneity of droughts

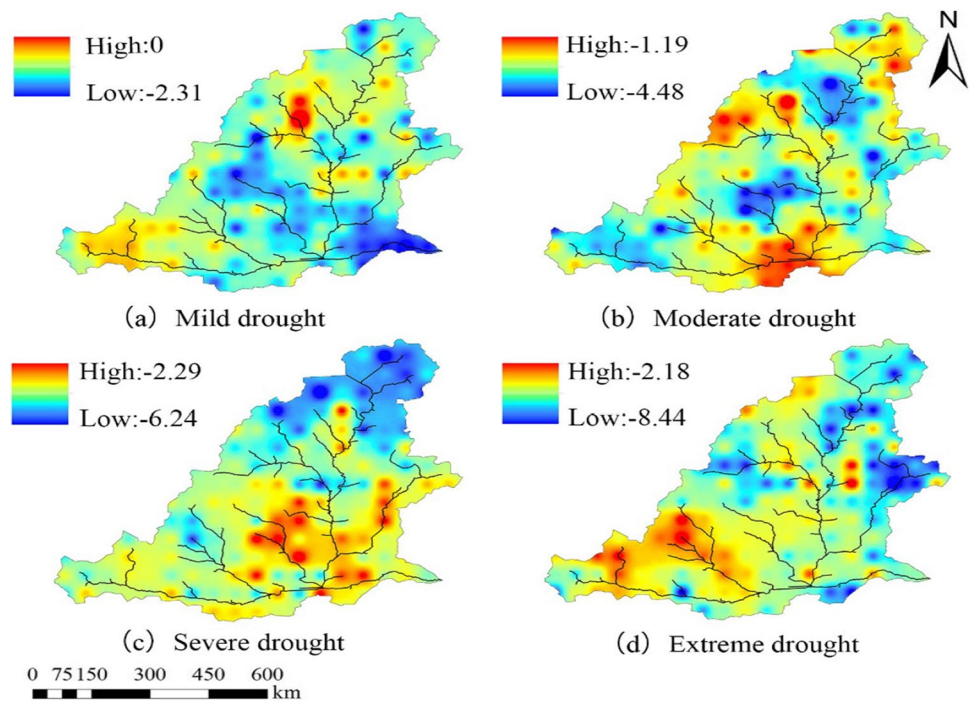
Global spatial correlation

The overall spatial correlation of drought frequency and intensity in the MYRB was calculated using the global Moran's I (Table 3). Moran's I was positive, and there was a positive spatial correlation between drought frequency and intensity. The frequencies of mild and severe droughts showed strong spatial dependence and clusters at the 99% confidence level. The four levels of drought intensity showed non-significant positive spatial correlations.

Local spatial correlation

The local spatial clustering characteristics of drought frequency (Fig. 11) and intensity (Fig. 12) were analyzed using the local Moran's I. High-high clustering (H-H) and low-low clustering (L-L) indicate homogeneity of drought frequency and intensity, that is, a positive spatial correlation was observed. High-low clustering (H-L) and low-high clustering (L-H) indicate heterogeneity,

Fig. 9 Spatial distribution of drought intensity in the MYRB from 1961 to 2019



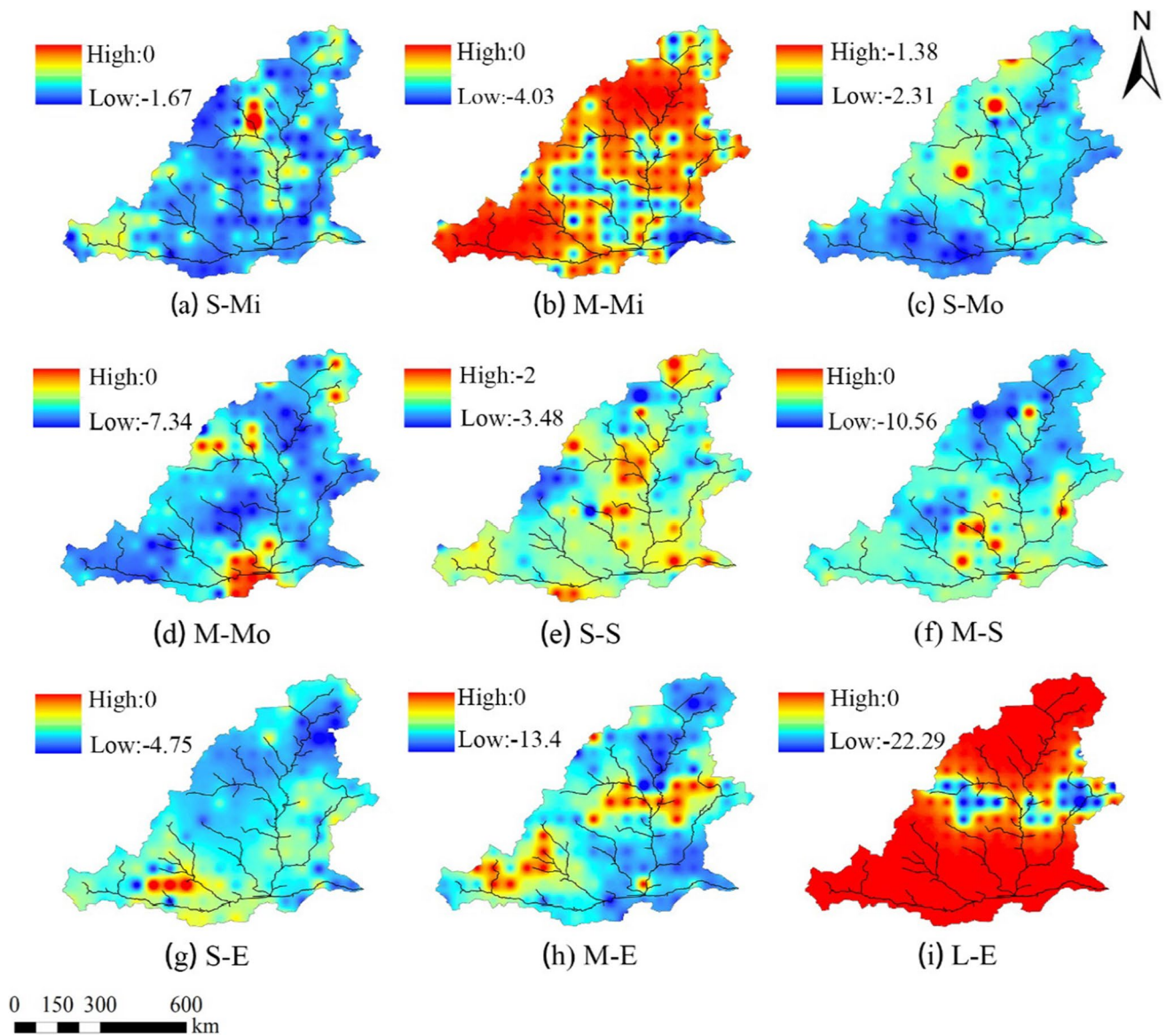


Fig. 10 Spatial distribution of drought intensity for different types of droughts (based on durations and grades) in the MYRB from 1961 to 2019

Table 3 The Moran’s index of drought frequency and intensity which was used to detect global spatial clusters and its variations in the study

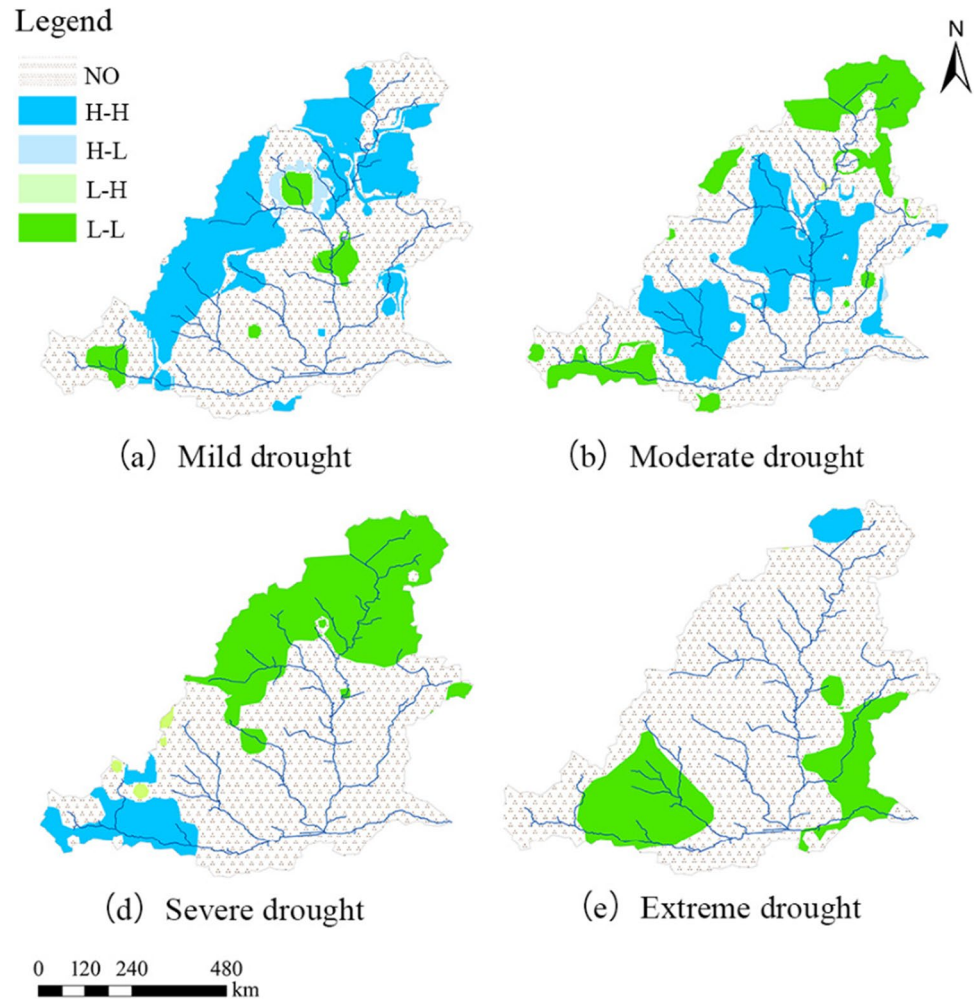
Value	Drought characteristics	Mild drought	Moderate drought	Severe drought	Extreme drought
I	Drought frequency	0.6537*	0.1857*	0.5514*	0.2747*
	Drought intensity	0.3168*	0.3572	0.1469*	0.3597

*A significant correlation at the 99% confidence level.

that is, a negative spatial correlation was observed. The spatial clustering characteristics of drought frequency and intensity varied between drought levels. Overall, spatial clustering characteristics were homogeneous, with a positive spatial correlation and strong spatial dependence.

The frequency of mild droughts was mainly as H–H clusters, which were concentrated in the western and northern parts of the MYRB, while L–L clusters were distributed in the central and southwestern parts of the MYRB. The spatial distribution of the frequency of mild droughts was generally homogeneous (Fig. 11a). The

Fig. 11 Local spatial clustering characteristics of the frequencies of different drought levels. High–high clusters: high values in a high-value neighborhood; low–low clusters: low values in a low-value neighborhood; low–high outliers: a low value in a high-value neighborhood; high–low outliers: a high value in a low-value neighborhood



distribution range of H–L and L–H clustering was relatively small and mainly distributed in the northwestern region. The H–H clustering of the frequency of moderate droughts was mainly distributed in the Jinghe and Wudinghe basins, while the L–L clustering was mainly distributed in the northern and southwestern parts of the MYRB (Fig. 11b). The frequencies of severe droughts (Fig. 11c) and extreme droughts (Fig. 11d) mainly showed L–L clustering. Among them, the L–L clusters of the frequency of severe droughts were distributed in the northern part of the MYRB, while those of extreme droughts were mainly distributed in the Weihe and Fenhe basins.

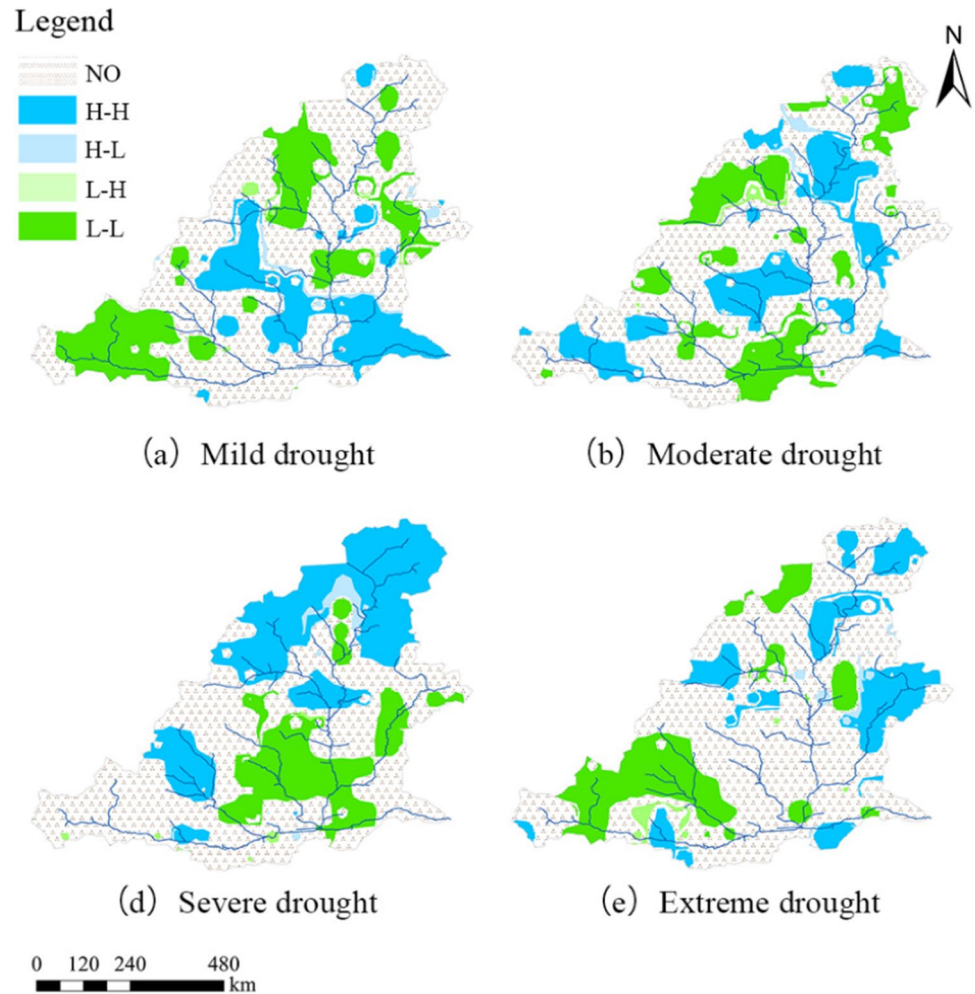
The H–H clustering of the intensity of mild droughts was distributed in the Luohe River basin and the southern part of the MYRB, while L–L clustering was distributed in the upper reaches of the Weihe, Wudinghe, and Fenhe basins (Fig. 12a). The H–H clusters of the intensity of moderate droughts were mainly distributed in the upper reaches of the Wudinghe River basin and the lower reaches of the Weihe and Luohe basins, while the L–L clusters were distributed in the upper reaches of the Weihe and Jinghe basins and in

the northern part of the MYRB (Fig. 12b). The H–H clusters of the intensity of severe droughts were distributed in the northern parts of the MYRB and in the upper reaches of the Jinghe River basin, while the L–L clusters were distributed in the Luohe and Fenhe basins (Fig. 12c). The H–H clusters of the intensity of extreme droughts were distributed in the northern part of the MYRB and in the Wudinghe River basin, while the L–L clusters were concentrated in the Weihe River basin (Fig. 12d).

Discussion

The spatiotemporal distribution characteristics of SPEI mainly reveal meteorological drought variations. By calculating the SPEI at different timescales based on the grid data of long timeseries, it was found that the SPEI decreased gradually after 1985. In other words, the trend of aridification in the MYRB intensified after 1985. The droughts in 1987 and 1997 were particularly severe, which was consistent with the findings of Han et al. (2021).

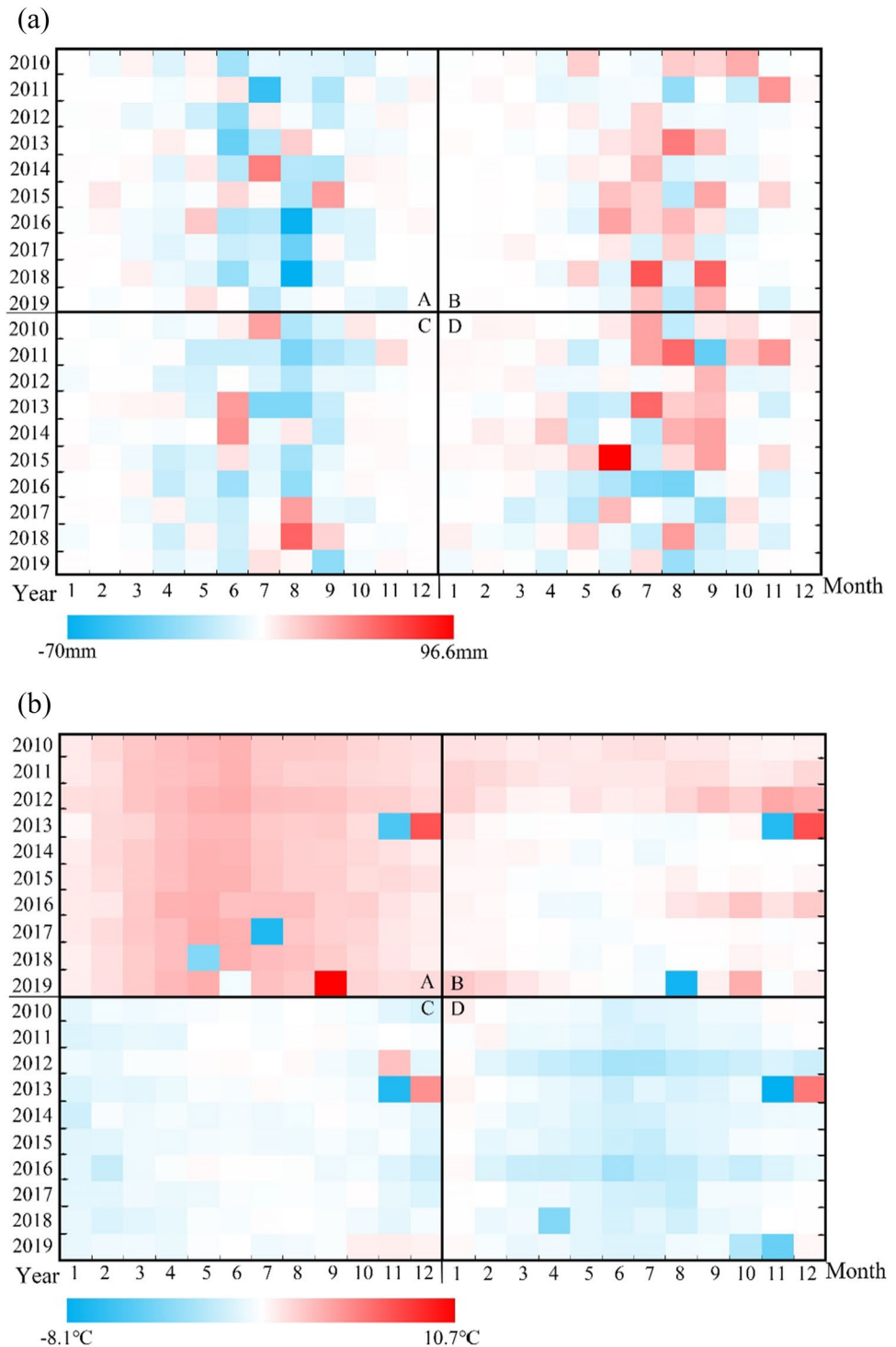
Fig. 12 Local spatial clustering characteristics of the intensities of different drought levels



Zhou et al. (2021) analyzed the spatiotemporal evolution of drought characteristics across the Yellow River basin and found that the SPEI decreased gradually after 1981, and decreased significantly ($p < 0.05$) in 1996. There is a 4-year error between the data in this paper and in his results. This study analyzed the spatiotemporal distribution characteristics of drought frequency and intensity; it was found that the frequency and intensity of droughts were higher in the south and lower in the north of the MYRB. Combined with the duration, it becomes apparent that the drought duration was longer and more serious in the northern part of the MYRB. Another conclusion of Zhou et al. (2021) was “The larger the time scale, the fewer the number of droughts,” which is consistent with the conclusion “The longer the drought event lasted, the lower the drought frequency and the drought intensity” of this study. The results of this study are consistent with the overall drought trends reported for other parts of China (Xu et al. 2015; Yu et al. 2014; Peng et al. 2019; Zeng et al. 2021) and can effectively reflect the drought situation in the MYRB.

Previous studies only considered the durations, frequencies, and intensities of different drought levels, while ignoring the frequencies and intensities of droughts with different durations, resulting in an incomplete analysis of the corresponding spatial distribution characteristics (Zhai et al. 2017; Huang et al. 2019). To achieve the goal of finely assessing the spatiotemporal characteristics of droughts in the study area, this study first analyzed the spatial distribution characteristics of the frequencies and intensities of different drought levels. Then, the frequencies, intensities, and durations of different drought levels were combined to achieve a refined representation of the corresponding spatial characteristics. The intensities of medium–long-term mild–moderate droughts were lower than those of short–medium-term severe–extreme droughts. For example, the intensity of a mild drought lasting 5 months was lower than that of a severe drought lasting 3 months. This, combined with the fact that the drought intensity value is negative, suggests that longer-duration low-level droughts may have a more serious impact on socioeconomic development. Therefore, while analyzing the frequencies and

Fig. 13 Difference between the monthly precipitation (temperature) data of four monitoring stations (A: Wuzhai; B: Hohhot; C: Xiji; D: Yaoxian) and the corresponding monthly precipitation (temperature) grid data (2010–2019). (a) Precipitation; (b) temperature



intensities of different drought levels, the drought duration grades must be considered to improve the accuracy of drought research and enhance the practical significance of drought research.

Figure 13 shows a comparison and analysis of the difference between site data and grid data for temperature and precipitation. The precipitation grid data were based on the

spatial interpolation of station precipitation to obtain smooth areal rainfall data. When heavy rainfall or rainstorms occur in a local area, spatial interpolation weakens the extreme value of precipitation to a certain extent, which may affect the results and accuracy of drought research. Affected by the summer monsoon, there are more heavy rainfall events in southeastern China than in other parts of China, and

the spatial variability of rainfall is relatively large, resulting in a relatively large error after interpolation. However, in inland areas of China, the possibility of heavy rainfall is relatively low, the precipitation changes are small, and the relative error is small (Zhao et al. 2014). The grid data used in this study were obtained from the China National Meteorological Center and are based on interpolation from ground-level national high-density stations with relatively high accuracy. To test the spatial interpolation accuracy of grid data, four national meteorological stations in the study area (Wuzhai, Hohhot, Xiji, and Yaoxian) were selected, and the station data and grid data of monthly precipitation during 2010–2019 were compared (Fig. 13a). When the difference between the station and grid data was > 0 , the extreme rainfall value was weakened; then, the difference was < 0 , and the grid data value was falsely high. The precipitation values at the four meteorological stations were generally lower than the grid precipitation values from June to September during 2010–2019 (Fig. 10). Compared with the precipitation data of the four stations, the falsely high precipitation months at the grid points of the stations at Wuzhai, Hohhot, Xiji, and Yaoxian accounted for 68.3%, 62.5%, 63.3%, and 48.3% of the total months, respectively. In August 2018, the falsely high precipitation value of the grid point where the Wuzhai monitoring station is located was the largest (70 mm). In June 2015, the weakened precipitation at the Yaoxian monitoring station was the largest (96.6 mm). Overall, the precipitation error between the four stations and the grids was larger from June to September, which may be related to the increase in the number of local extreme precipitation events caused by the summer monsoon. Only the month corresponding to weakening precipitation of extreme values at the Yaoxian monitoring station accounted for $< 50\%$ of the total months, which may be related to the terrain, latitude, and longitude. Thus, after the grid precipitation is interpolated based on station precipitation, there is a problem of weakening the extreme precipitation value or falsely high grid precipitation, which may affect the accuracy of drought research results. However, months with precipitation errors of < 10 mm between the four stations and the corresponding grids accounted for 75.8%, 72.5%, 73.3%, and 62.5% of the total months, respectively. Most precipitation errors at most stations and grids could be maintained within 10 mm. Overall, months with temperature errors of < 3 °C between the four stations and the corresponding grids accounted for 94.2%, 97.7%, 98.3%, and 94.2% of the total months, respectively (Fig. 13b). Compared with the temperature data of the four stations, the falsely high-temperature months at the grid points of the stations at Wuzhai and Hohhot accounted for 97.5% and 98.3% of the total months. The weakening extreme temperature value months at the grid points of the stations at Xiji and Yaoxian accounted for 96.7% and 98.3%

of the total months. It may be that the spatial variability of temperatures is relatively small, and the error between stations and grids is small. Over 94% temperature errors at stations and grids could be maintained within 3 °C. Therefore, the errors of stations and grids have little impact on the drought research results. Ahmadalipour and Moradkhani (2017) used station data to analyze meteorological and hydrological droughts in the Yellow River basin from 1961 to 2015 and found that the drought trend increased, with particularly serious droughts occurring in 1997, 1999, 2002, and 2003. Bao et al. (2019) analyzed the climate variability in the MYRB from 1956 to 2016 using station data and showed that the MYRB became drier during this period. Huo et al. (1998) reported an abnormal decrease in precipitation and abnormal increase in aridity during the flood season in the Yellow River basin in 1997, whereby the flow cut off was 226 days. Using grid data, the present study found that the SPEI exhibited a downward trend from 1961 to 2019 and that the lowest SPEI occurred in 1997; thus, it was considered to be a typical drought year. This result was consistent with the conclusions drawn by Ahmadalipour and Moradkhani (2017) and Bao et al. (2019) based on meteorological station data. In recent years, scholars have focused long-series, high-precision, and wide-coverage data, and the use of grid data has become a research trend. In addition to the above advantages, grid data can also allow the spatiotemporal characteristics of drought to be effectively analyzed, thus justifying the use of grid data as the basic data in this study.

In recent years, scholars have realized that drought events are three-dimensional spatial structures; therefore, many three-dimensional algorithms have been developed. Among these, a three-dimensional clustering algorithm has been continuously innovated and developed. It combines the longitude, latitude, time, and space of drought events to dynamically describe the spatiotemporal evolution of drought conditions (Zhu et al. 2019). Based on three-dimensional clustering algorithms, methods such as severity–area–duration and intensity–area–duration have been continuously developed (Mathbout et al. 2017; Liu et al. 2019). Scholars are increasingly inclined to diversify characteristic variables and refine spatial representations to improve the accuracy associated with the analysis of the spatiotemporal characteristics of drought events (Xu et al. 2021a, b; Rashid et al. 2018). In this study, only the drought frequency, intensity, and duration were considered. In the future, other characteristic indicators, such as centroids, track path, and propagation direction, will be added to analyze meteorological droughts more comprehensively. In addition, we will explore ways to improve the accuracy of meteorological grid data and reduce the uncertainty of extreme climate research.

Conclusions

Using $0.5^{\circ} \times 0.5^{\circ}$ monthly precipitation and temperature grid data for the MYRB from 1961 to 2019, the SPEI was calculated for different timescales, and the spatiotemporal characteristics of different drought levels were analyzed. The conclusions are as follows:

- (1) From 1961 to 2019 in the MYRB, the SPEI decreased at a rate of $-0.1145/\text{decade}$. Seasonally, the SPEI decreased at a rate of $-0.1356/\text{decade}$, $-0.0362/\text{decade}$, and $-0.0745/\text{decade}$ in spring, summer, and autumn, respectively, whereas it increased at a rate of $0.0781/\text{decade}$ in winter. The M–K mutation test showed that there were significant mutation points in the SPEI both annually and in spring, autumn, and winter; however, no mutation points were observed in summer. The mutation curves for 2000–2002, 2004–2019, spring during 1961–1965, spring during 1973–1977, summer during 1987–2011, and winter in 1979 passed the 0.05 significance test, showing significant downward trends.
- (2) There were significant spatial differences in the frequencies and intensities of different drought levels. The frequencies of mild and moderate droughts were relatively high. The highest frequency of moderate droughts was 79. The highest frequency of mild droughts was observed in the periphery area of the MYRB, while low intensity droughts were concentrated in the southeast. The frequency of moderate droughts was mainly concentrated in the Wudinghe and Jinghe basins, which was consistency with the intensity distribution of moderate droughts. The frequency and intensity of severe droughts decreased from the south to the north. The frequency of extreme droughts was mainly concentrated in the Wudinghe River basin and in the northern part of the MYRB, with the high-intensity area being the Fenhe River basin.
- (3) The spatial distributions of the frequencies and intensities of different types of droughts were generally consistent. The duration of 93.5% of drought events was short term, and only extreme droughts had a long-term duration. The longer the drought event lasted, the lower the drought frequency and the lower the drought intensity. For short-term droughts, the highest frequency was observed for S-Mo droughts, reaching 78, which had the lowest intensity of -2.31 . For medium-term droughts, the highest frequencies were observed for M-Mo and M-S droughts, reaching eight, which had the lowest intensities of -7.34 and -10.56 , respectively. For L-E droughts, the highest frequency was one, while the lowest intensity was -22.29 .

- (4) Drought frequency was mainly manifested in spatial clusters and a random distribution, and the spatial clusters of the frequencies of mild and extreme droughts were the most significant. The high frequencies of mild and moderate droughts were clustered in the western and central parts of the MYRB, respectively. The low frequencies of severe and extreme droughts were clustered in northern and southwestern MYRB, respectively. The drought intensity mainly showed non-significant spatial clustering and a random distribution. The agglomeration regularity of the high and low drought intensities was poor; however, the high and low values of drought intensity were concentrated in the middle and upper reaches of each tributary.

These research results provide reference for disaster prevention and mitigation, agricultural production planning, and water resource allocation in the MYRB. In future research, we will add other characteristic indicators and explore ways to improve the accuracy of meteorological grid data.

Acknowledgements We acknowledge the use of data from the National Meteorological Information Centre of the Chinese Meteorological Administration (<http://cdc.nmic.cn>) and Geospatial Data Cloud (<http://www.gscloud.cn>).

Author contribution Ying Li: conceptualization; formal analysis; supervision; roles/writing—original draft; writing—review and editing. Chenchen Jia: data curation; methodology; visualization; roles/writing—original draft; writing—review and editing. Shuang Ma: methodology; resources; visualization; writing—review and editing. Zhentai Hu: data curation; software; visualization; writing—review and editing. Jin Sun: resources; software; validation; writing—review and editing.

Funding This research was funded by National Natural Science Foundation of China (grant number 52079060) and Liaoning Revitalization Talents Program.

Data availability Not applicable.

Declarations

Ethics approval and consent to participate Not applicable.

Consent for publication Not applicable.

Conflict of interest The authors declare no competing interests.

References

- Ahmadalipour A, Moradkhani H (2017) Analyzing the uncertainty of ensemble-based gridded observations in land surface simulations and drought assessment. *J Hydrol* 555:557–568. <https://doi.org/10.1016/j.jhydrol.2017.10.059>

- Arshad A, Zhang W, Zhang Z, Wang S, Zhang B, Cheema M, Shalamzari M (2021) Reconstructing high-resolution gridded precipitation data using an improved downscaling approach over the high altitude mountain regions of Upper Indus Basin (UIB). *Sci Total Environ* 784:147140. <https://doi.org/10.1016/j.scitotenv.2021.147140>
- Ayantobo OO, Yi L, Song S, Yao N (2017) Spatial comparability of drought characteristics and related return periods in mainland China over 1961–2013. *J Hydrol* 550:549–567. <https://doi.org/10.1016/j.jhydrol.2017.05.019>
- Bao Z, Zhang J, Wang G, Chen Q, Guan T, Yan X et al (2019) The impact of climate variability and land use/cover change on the water balance in the Middle Yellow River Basin. *China. J Hydrol* 577:123942
- Chen Y, Fu B, Zhao Y, Wang K, Zhao M, Ma J et al (2020) Sustainable development in the Yellow River Basin: issues and strategies. *J Clean Prod* 263:121223. <https://doi.org/10.1016/j.jclepro.2020.121223>
- Cook BI, Ault TR, Smerdon JE (2015) Unprecedented 21st century drought risk in the American Southwest and Central Plains. *Sci Adv* 1(1):e1400082. <https://doi.org/10.1126/sciadv.1400082>
- Giorgi F (2008) Regionalization of climate change information for impact assessment and adaptation. *Bull World Meteorol Organization* 57(2):86–92. <https://doi.org/10.1002/joc.4036>
- Guo E, Liu X, Zhang J, Wang Y, Wang C, Wang R, Wang D (2017) Assessing spatiotemporal variation of drought and its impact on maize yield in Northeast China. *J Hydrol* 553:231–247. <https://doi.org/10.1016/j.jhydrol.2017.07.060>
- Han Z, Huang Q, Huang S, Leng G, Bai Q, Liang H et al (2021) Spatial-temporal dynamics of agricultural drought in the Loess Plateau under a changing environment: characteristics and potential influencing factors. *Agric Water Manag* 244:106540. <https://doi.org/10.1016/j.agwat.2020.106540>
- Hao Z, Aghakouchak A, Nakhjiri N, Farahmand A (2014) Global integrated drought monitoring and prediction system. *Scientific Data* 1:140001. <https://doi.org/10.1038/sdata.2014.1>
- Hisdal H, Tallaksen LM, Clausen B, Peters E, Gustard A (2004) Hydrological drought characteristics. *Dev Water Sci* 48:139–198
- Hong M, Lee SH, Lee SJ, Choi JY (2021) Application of high-resolution meteorological data from NCAM-WRF to characterize agricultural drought in small-scale farmlands based on soil moisture deficit. *Agric Water Manag* 243:106494. <https://doi.org/10.1016/j.agwat.2020.106494>
- Hu Y, Zhou B, Han T, Li H, Wang H (2021) Out-of-phase decadal change in drought over northeast china between early spring and late summer around 2000 and its linkage to the Atlantic Sea surface temperature. *J Geophys Res Atmos* 126(9):e2020JD034048. <https://doi.org/10.1029/2020JD034048>
- Huang S, Wang L, Wang H, Huang Q, Leng G, Fang W, Zhang Y (2019) Spatio-temporal characteristics of drought structure across China using an integrated drought index. *Agric Water Manag* 218:182–192. <https://doi.org/10.1016/j.agwat.2019.03.053>
- Huang S, Wang L, Wang H, Huang Q, Leng G, Fang W, Zhang Y (2019) Spatio-temporal characteristics of drought structure across China using an integrated drought index. *Agric Water Manag* 218:182–192. <https://doi.org/10.1016/j.agwat.2019.03.053>
- Huo S, Wang H, Peng M (1998) Analysis on no-flow in the lower Yellow River in 1997. *Yellow River* 20(1):1–3 (In Chinese)
- Kim W, Iizumi T, Nishimori M (2019) Global patterns of crop production losses associated with droughts from 1983 to 2009. *J Appl Meteorol Climatol* 58(6):1233–1244. <https://doi.org/10.1175/JAMC-D-18-0174.1>
- Kumari M, Sarma K, Sharma R (2019) Using Moran's I and GIS to study the spatial pattern of land surface temperature in relation to land use/cover around a thermal power plant in Singrauli district, Madhya Pradesh, India. *Remote Sens Appl Soc Environ* 15:100239. <https://doi.org/10.1016/j.rsase.2019.100239>
- Lhotka O, Trnka M, Kyselý J, Markonis J, Baiek J, Možný M (2020) Atmospheric circulation as a factor contributing to increasing drought severity in central Europe. *J Geophys Res Atmos* 125(18):e2019JD032269. <https://doi.org/10.1029/2019JD032269>
- Li J, Wang J, Zhang J, Zhang J, Kong H (2021) Dynamic changes of vegetation coverage in China-Myanmar economic corridor over the past 20 years. *Int J Appl Earth Obs Geoinf* 102:102378. <https://doi.org/10.1016/j.jag.2021.102378>
- Liu Y, Zhu Y, Ren L, Singh V, Yong B, Jiang S, Fei Y, Yang X (2019) Understanding the spatiotemporal links between meteorological and hydrological droughts from a three-dimensional perspective. *J Geophys Res Atmos* 124(6):3090–3109. <https://doi.org/10.1029/2018JD028947>
- Mathbout S, Lopez-Bustins J, Martin-Vide J, Bech J, Rodrigo F (2017) Spatial and temporal analysis of drought variability at several time scales in Syria during 1961–2012. *Atmos Res* 200:153–168. <https://doi.org/10.1016/j.atmosres.2017.09.016>
- McKee TB, Doesken NJ, Kleist J (1993) The relationship of drought frequency and duration to time scales. *Proceedings of the 8th Conference on Applied Climatology* 17(22):179–183
- Mishra AK, Singh VP (2010) A review of drought concepts. *J Hydrol* 391(1–2):202–216. <https://doi.org/10.1016/j.jhydrol.2010.07.012>
- Omer A, Ma Z, Zheng Z, Saleem F (2020) Natural and anthropogenic influences on the recent droughts in Yellow River Basin. *China Science of the Total Environment* 704:135428. <https://doi.org/10.1016/j.scitotenv.2019.135428>
- Pachauri RK, Reisinger A (2007) IPCC fourth assessment report. IPCC, Geneva
- Palmer WC (1965) Meteorological drought. US Department of Commerce, Weather Bureau 1965
- Palmer WC, Wayne C (1968) Keeping track of crop moisture conditions, nationwide: the new crop moisture index. *Weatherwise* 21(4):156–161. <https://doi.org/10.1080/00431672.1968.9932814>
- Peng SM, Zheng XK, Wang Y, Li K (2019) Synergetic optimal operation of cascade reservoirs in mainstream of Yellow River responding to drought. *Energy Procedia* 158:6288–6295. <https://doi.org/10.1016/j.egypro.2019.01.445>
- Prudhomme C, Giuntoli I, Robinson E, Clark D, Arnell N, Dankers R et al (2014) Hydrological droughts in the 21st century, hotspots and uncertainties from a global multimodel ensemble experiment. *Proc Natl Acad Sci* 111(9):3262–3267. <https://doi.org/10.1073/pnas.1222473110>
- Rajsekhar D, Singh VP, Mishra AK (2015) Integrated drought causality, hazard, and vulnerability assessment for future socioeconomic scenarios: an information theory perspective. *J Geophys Res Atmos* 120(13):6346–6378. <https://doi.org/10.1002/2014JD022670>
- Rashid MM, Johnson F, Sharma A (2018) Identifying sustained drought anomalies in hydrological records: a wavelet approach. *J Geophys Res Atmos* 123(14):7416–7432. <https://doi.org/10.1029/2018JD028455>
- Son B, Park S, Im J, Park S, Ke Y, Quackenbush L (2021) A new drought monitoring approach: vector projection analysis (VPA). *Remote Sens Environ* 252:112145. <https://doi.org/10.1016/j.rse.2020.112145>
- Sun H, Zhao X, Chen Y, Gong A, Yang J (2013) A new agricultural drought monitoring index combining MODIS NDWI and day-night land surface temperatures: a case study in China. *Int J Remote Sens* 34(24):8986–9001. <https://doi.org/10.1080/01431161.2013.860659>
- Tirivarombo S, Osupile D, Eliasson P (2018) Drought monitoring and analysis: standardised precipitation evapotranspiration index (SPEI) and standardised precipitation index (SPI). *Phys Chem Earth* 106:1–10. <https://doi.org/10.1016/j.pce.2018.07.001>
- Vicente-Serrano SM, Beguería S, López-Moreno JI (2010) A multiscale drought index sensitive to global warming: the standardized

- precipitation evapotranspiration index. *J Clim* 23(7):1696–1718. <https://doi.org/10.1175/2009JCLI2909.1>
- Wang H, Chen Y, Pan Y, Li W (2015) Spatial and temporal variability of drought in the arid region of China and its relationships to teleconnection indices. *J Hydrol* 523:283–296. <https://doi.org/10.1175/2009JCLI2909.1>
- World Meteorological Organization (WMO) (2007) United nations environment programme (UNEP): scientific assessment of ozone depletion: 2006, WMO, Geneva, Switzerland
- World Meteorological Organization (WMO) (2019) Extreme-scale computing and data handling - the heart of progress in weather and climate prediction: 2018, WMO, Geneva, Switzerland
- World Meteorological Organization (WMO) (2020) The Atlas of mortality and economic losses from weather, climate and water extremes (1970–2019), WMO, Geneva, Switzerland
- Wu J, Miao C, Zheng H, Duan Q, Lei X, Li H (2018) Meteorological and hydrological drought on the Loess Plateau, China: evolutionary characteristics, impact, and propagation. *J Geophys Res Atmos* 123(20):11569–11584. <https://doi.org/10.1029/2018JD029145>
- Wang Y, Wang S, Zhao W., Liu Y (2021) The increasing contribution of potential evapotranspiration to severe droughts in the Yellow River basin. *J Hydrol* 127310. <https://doi.org/10.1016/j.jhydrol.2021.127310>
- Xu C, Guan Q, Lin J, Luo H, Yang L, Tan Z (2020) Spatiotemporal variations and driving factors of dust storm events in northern China based on high-temporal-resolution analysis of meteorological data (1960–2007). *Environ Pollut* 260:114084. <https://doi.org/10.1016/j.envpol.2020.114084>
- Xu K, Yang D, Yang H, Li Z (2015) Spatio-temporal variation of drought in China during 1961–2012: a climatic perspective. *J Hydrol* 526:253–264. <https://doi.org/10.1016/j.envpol.2020.114084>
- Xu Y, Zhang X, Hao Z, Hao F, Li C (2021a) Projections of future meteorological droughts in China under CMIP6 from a three imensional perspective. *Agric Water Manag* 252:106849. <https://doi.org/10.1016/j.agwat.2021.106849>
- Xu Z, Zhang S, Yang X (2021b) Water and sediment yield response to extreme rainfall events in a complex large river Basin: a case study of the Yellow River Basin. *China J Hydrol* 597(2):126183. <https://doi.org/10.1016/j.jhydrol.2021.126183>
- Yang Y, Sun L, Guo C (2018) Aero-Material consumption prediction based on linear regression model. *Procedia Comput Sci* 131:825–831. <https://doi.org/10.1016/j.procs.2018.04.271>
- Yerdelen C, Abdelkader M, Eris E (2021) Assessment of drought in SPI series using continuous wavelet analysis for GEDIZ Basin Turkey. *Atmos Res* 260:105687. <https://doi.org/10.1016/j.atmosres.2021.105687>
- Yu M, Li Q, Hayes MJ, Svoboda MD, Heim RR (2014) Are droughts becoming more frequent or severe in China based on the standardized precipitation evapotranspiration index: 1951–2010? *Int J Climatol* 34(3):545–558. <https://doi.org/10.1002/joc.3701>
- Yuan Y, Cave M, Zhang C (2018) Using local Moran's I to identify contamination hotspots of rare earth elements in urban soils of London. *Appl Geochem* 88:167–178. <https://doi.org/10.1016/j.apgeochem.2017.07.011>
- Zeng P, Sun F, Liu Y, Wang Y, Li G, Che Y (2021) Mapping future droughts under Global warming across China: a combined multi-timescale meteorological drought index and SOM-Kmeans approach. *Weather Clim Extremes* 31:100304. <https://doi.org/10.1016/j.wace.2021.100304>
- Zhai J, Huang J, Su B, Cao L, Wang Y, Jiang T, Fischer T (2017) Intensity-area-duration analysis of droughts in China 1960–2013. *Clim Dyn* 48(1–2):151–168. <https://doi.org/10.1007/s00382-016-3066-y>
- Zhang Q, Yu H, Sun P, Singh VP, Shi P (2019) Multisource data based agricultural drought monitoring and agricultural loss in China. *Global Planet Change* 172:298–306. <https://doi.org/10.1016/j.gloplacha.2018.10.017>
- Zhao H, Gao G, An W, Zou X, Hou M (2017) Timescale differences between SC-PDSI and SPEI for drought monitoring in China. *Physics and Chemistry of the Earth, Parts a/b/c* 102:48–58. <https://doi.org/10.1016/j.pce.2015.10.022>
- Zhao J, Li C, Yang T, Tang Y, Yin Y, Luan X, Sun S (2020) Estimation of high spatiotemporal resolution actual evapotranspiration by combining the SWH model with the METRIC model. *J Hydrol* 586:124883. <https://doi.org/10.1016/j.jhydrol.2020.124883>
- Zhao Y, Zhu J, Xu Y (2014) Establishment and assessment of the grid precipitation datasets in China for recent 50 years. *J Meteorol Sci* 143:845–863 (In Chinese)
- Zhou K, Wang Y, Chang J, Zhou S, Guo A (2021) Spatial and temporal evolution of drought characteristics across the Yellow River basin. *Ecol Ind* 131:108207. <https://doi.org/10.1016/j.ecolind.2021.108207>
- Zhu Y, Liu Y, Wang W, Singh V, Ma X, Yu Z (2019) Three dimensional characterization of meteorological and hydrological droughts and their probabilistic links. *J Hydrol* 578:124016. <https://doi.org/10.1016/j.jhydrol.2019.1240>

Publisher's note Springer Nature remains neutral with regard to jurisdictional claims in published maps and institutional affiliations.